Geophysical Journal International

Geophys. J. Int. (2015) **203,** 228–242
GJI Geodynamics and tectonics

doi: 10.1093/gji/ggv294

Ground motions induced by a producing hydrocarbon reservoir that is overlain by a viscoelastic rocksalt layer: a numerical model

G. Marketos, R. Govers and C.J. Spiers

Geosciences Department, Utrecht University, The Netherlands. E-mail: g.marketos@uu.nl

Accepted 2015 July 13. Received 2015 July 13; in original form 2015 March 4

SUMMARY

Hydrocarbon reservoir pressure depletion leads to stress changes inside the reservoir and ground deformation which is registered at the surface as subsidence. As reservoirs are often overlain by layers of rocksalt (or other evaporites), which are materials that flow so as to relax stresses inside them, there is the potential for time-varying surface subsidence. This work focuses on understanding the macroscopic mechanisms that lead to rocksalt flow-induced ground displacements. A Finite Element Model is used for this purpose in which the rocksalt layer is represented by a viscoelastic Maxwell material. Two distinct mechanisms that lead to displacement are observed. These are active during different stages of the deformation and have different timescales associated with them. An important observation is that the timescale for deformation that is measured at the ground surface is not equal to the timescale for deformation of a viscoelastic material element, but can be many times larger than that. The sensitivity of the response to the thickness and location of the rocksalt layer is also presented. Conclusions are drawn which allow for the relative importance of the presence of the rocksalt layer to be assessed and for a framework for understanding time-dependent subsidence above producing hydrocarbon reservoirs to be developed. Finally the changes in stress distribution around a producing reservoir are also briefly discussed.

Key words: Numerical solutions; Geomechanics; Creep and deformation; Mechanics, theory and modelling.

1 INTRODUCTION

Production from hydrocarbon reservoirs causes reservoir compaction that is registered at the surface as subsidence. The link between pore pressure changes at the reservoir level and surface subsidence is well known (e.g. Nagel 2001; Gambolati *et al.* 2006; Vasco *et al.* 2008; Ketelaar 2009). However, there is growing evidence to suggest that there is a delay in the subsidence response, that is a time-dependence of ground deformations (see Hettema *et al.* 2002). A number of processes have been proposed to explain how pore pressure decrease can lead to the observed time-dependent subsidence (see Hettema *et al.* 2002)—examples include continuing compaction at the reservoir level due to the increase in effective stresses or changes in pore-fluid composition, delayed compaction of the surrounding layers due to pore pressure equilibration, reservoir rock creep (e.g. Hol *et al.* 2015) and shear-stress-induced flow inside evaporite cover layers (e.g. rocksalt, a material that deforms at timescales relevant to the problem when shear stresses are applied to it). This latter hypothesis will be tested here.

The focus here on the stress-induced rocksalt flow mechanism is motivated by the observation that a number of hydrocarbon reservoirs are overlain by relatively thick layers of rocksalt, which act as caprocks. Grunau (1981) states that 'about 62 per cent of the caprock seals for the world's 176 giant gas fields are shales and about 38 per cent are evaporites'. While this might not fully reflect the current situation, it is indicative. The more recent work of Mohriak *et al.* (2012) also makes the link between reservoirs and evaporite caps for large hydrocarbon fields offshore Brazil and stresses the importance of such fields on total hydrocarbon production. Montgomery & Moore (1997) do the same for the Gulf of Mexico stating that 'exploration for deep-water sandstone reservoirs beneath allochthonous salt in the Gulf of Mexico represents a major new frontier play in North America'. Other examples of subsalt reservoirs include the gas fields in the Netherlands (see NAM 2013), in China (see Yu *et al.* 2014) or Oman (see Schoenherr *et al.* 2007) to name but a few. The salt layers in these locations are relatively thick and can range to over 400 m in places. In addition, rocksalt layers are present in a large number of other areas (see e.g. Lefond 1969 for an overview), and there is always the potential for discovery of new hydrocarbon reservoirs beneath them as hinted by Mohriak *et al.* (2012) for example.

Even though the presence of a rocksalt layer above reservoirs is very common, no study has fully assessed the significance of stress-induced viscous rocksalt flow on ground deformation. For example, the mechanisms by which the stresses relax and the magnitude, spatial extent and timescale of the stress redistribution remain unclear. It is also unknown what the resultant pattern of deformation is, and whether this can result in deformations that are detectable at the

ground surface. This last point is especially important for low lying regions such as the Netherlands where subsidence predictions need to be as accurate as possible. The current study aims to fill this gap; a literature review of relevant modelling work will first be presented and then results of simulations conducted will be discussed with the aim of providing a framework for understanding time-dependent ground deformations above a producing hydrocarbon reservoir as induced by stress relaxation inside a rocksalt layer. It should also be noted that results presented here might be relevant to the study of phenomena in which a cavity or forcing region exists or is being created in a region in the vicinity of an evaporitic (or other viscous) layer. Geologists or engineers working on such problems will therefore find the conclusions drawn from this study useful.

2 PREVIOUS ATTEMPTS TO MODELLING PRODUCTION-INDUCED GROUND DEFORMATION

The starting point for modelling production-induced ground deformation around a hydrocarbon reservoir is to assume that all deformation is instantaneous, that is, that the ground is elastic. This is common also for other problems that involve underground cavities, such as magmatic chambers that inflate or deflate (e.g. Mogi 1958 with a small typo, Yoshikawa 1961), underground tunnels when constructed (see e.g. Verruijt 1996; Zymnis *et al.* 2013; Pinto & Whittle 2014) and underground cavities that collapse. For relatively simple cavity (or reservoir) geometries and boundary conditions inside uniform elastic half-spaces, analytical solutions for rock mass and ground surface displacements exist (see e.g. Segall 2010 for a review).

Elastic solutions have been used in the context of a subsiding reservoir, notably by Geertsma (1973) and Geertsma & van Opstal (1973). Fokker & Orlic (2006) have taken elastic analyses one step further. Faced with the problem of reservoirs of complex shape they superposed elastic solutions for point sources and point forces inside elastic full-spaces with their mirror images in order to match observed subsidence data. Such elastic methods are valuable as they provide a framework for understanding and roughly calculating ground deformation patterns at a given time instant. However, they do not offer insight into how ground deformation and surface subsidence evolve with time as they do not explicitly include time-dependent deformation. One way to do this is to extend elastic solutions so that they include viscoelasticity (Fokker & Orlic 2006). Muntendam-Bos *et al.* (2008) have used Fokker & Orlic's (2006) viscoelastic solution superposition method with a suitable inversion scheme to find the set of sources that provides the best possible match to a specific time-dependent subsidence measurement. These techniques work well but the focus is on matching already-observed response. An understanding of the mechanisms leading to the time-dependent deformations has not been addressed by the authors leaving a gap to be filled by the present study.

Other relevant work has been carried out using the Finite Element Method and has included a viscoelastic layer to represent a salt layer. In the work of Fokker *et al.* (1995) and Breunese *et al.* (2003), surface subsidence above a solution-mined rocksalt cavity is calculated. This means that the cavity whose shrinkage drives the deformation is located within the viscoelastic layer and not below it as is the case of evaporite-capped reservoirs (the case for this study), and so shear stress distributions within the evaporite and resultant ground deformation patterns will be different. Orlic & Wassing (2013) place the viscoelastic layer on top of the model reservoir but analyse stress redistributions due to reservoir depletion, without addressing ground motion in detail. Orlic *et al.* (2011) also consider reservoirs that undergo pore pressure changes and are overlain by a viscoelastic layer, but again focus on stress redistribution and use realistic but more complex subsurface geometries. Finally there is the on-going work by NAM (see e.g. NAM 2013) which uses complex geomechanical models intended to provide an as-accurate-as-possible prediction of surface subsidence but gives few details of the modelling choices made.

In the above-mentioned analyses, a solution for a specific location has been calculated. Complexity however makes it impossible to attribute aspects of the observed response to a specific component present in the model. In this study, we seek to find relations and trends that are generic and applicable to a wide range of actual reservoirs. We further seek to build up a good understanding of the mechanisms that lead to ground deformation as induced by viscous relaxation and flow inside a rocksalt layer. Another aim is to identify the dependence of the response on specific aspects that are relevant to the process (e.g. salt layer geometry, salt viscosity). As the target is to isolate the effect of rocksalt flow on the observed deformations, the surrounding rock layers will be modelled in a simplified manner, that is, as isotropic and elastic. Further complexities such as the presence of faults will be neglected.

3 METHOD

The mechanical equilibrium equations for the model reservoir are solved here using a Finite Element technique. The Lagrangian code GTecton (Govers & Wortel 1993) is used. GTecton iteratively solves the matrix equations (Govers & Wortel 2005). The code has been shown to be accurate for a wide range of elastic and viscoelastic problems, e.g. the simple viscoelastic problem described in Gerya (2010). Marketos & Govers (in preparation) discuss the accuracy of GTecton and a range of analytical models specifically for problems involving a pressurized cavity in a viscoelastic half-space. Non-linearity arising from geometry change is accounted for using a residual force update technique (Hall-Wallace & Melosh 1994; Govers & Wortel 1999).

Isotropic elasticity is assumed for all materials apart from the rocksalt. Rocksalt is modelled as an isotropic viscoelastic Maxwell material. An element of the Maxwell material can be represented as a spring and a dashpot in series (see e.g. Ranalli 1995). Such materials are characterized by the ratio of their shear viscosity to their shear modulus, which has units of time, and is termed Maxwell time τ. When a sudden strain is applied to an element of a Maxwell material the stress tends asymptotically to a new value. The difference between the current and final stresses then follows an exponential decay and the Maxwell time represents the time at which the stress difference has reached 1/e (i.e. 36.8 per cent) of its final value. Hence, the Maxwell time is a descriptor of how fast flow occurs inside the material and will be used in this work to non-dimensionalize time. The total strain rate for the Maxwell material under 2-D plane strain conditions is the sum of the elastic and viscous strain rate (Melosh & Raefsky 1980)

$$\begin{aligned}
\dot{\varepsilon}_{xx} &= \frac{1+\nu}{E}\left((1-\nu)\dot{\sigma}_{xx} - \nu\dot{\sigma}_{yy}\right) + \frac{\sigma_{xx}-\sigma_{yy}}{4\eta} \\
\dot{\varepsilon}_{yy} &= \frac{1+\nu}{E}\left((1-\nu)\dot{\sigma}_{yy} - \nu\dot{\sigma}_{xx}\right) - \frac{\sigma_{xx}-\sigma_{yy}}{4\eta} \\
\dot{\varepsilon}_{xy} &= \frac{1+\nu}{E}\dot{\sigma}_{xy} + \frac{\sigma_{xy}}{2\eta}
\end{aligned} \tag{1}$$

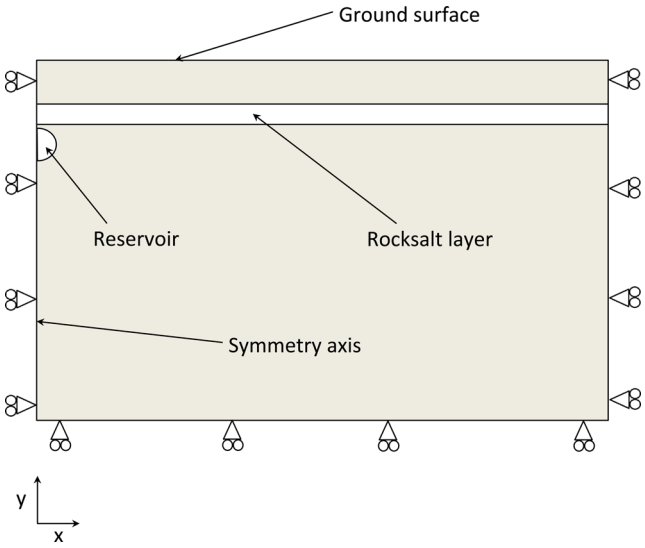

Figure 1. A sketch of the geometry for the Finite Element analyses presented here (not to scale).

where E, υ, η are the material Young's modulus, Poisson ratio, and viscosity, respectively, and σ and ε are the stress and strain respectively with a $\bullet$ over the symbol signifying the rate of change with time. Note that the above equations revert to the ones for an elastic material for infinite material viscosity.

4 MODEL SETUP

The geometry of the problem treated here is shown in Fig. 1. This consists of horizontal layers of isotropic elastic materials that represent the reservoir, the overburden and the basement rock, and a layer of an isotropic viscoelastic Maxwell material that represents the rocksalt layer (the cap rock). The modelling is performed in 2-D, and plane strain conditions are assumed. We have conducted analyses of similar geometries under 2-D axisymmetric conditions, the results and conclusions for which are very similar (see Marketos *et al.* 2015). As the problems investigated here are symmetric with respect to the vertical, only half the problem is modelled and mirror symmetry is used. The top surface (the line at $y = 0$) is set to be completely stress free, and the bottom and side boundaries have the displacement perpendicular to them set to zero. These are essentially mirror boundaries, but as they are at locations where the displacements would be very small anyway the effect of their presence on results becomes negligible. Both the effect of the location of the boundaries (here at $x = 64$ km and $y = -48$ km, respectively) and of the coarseness of the mesh has been investigated and results shown here are for meshes that are fine and extend far enough so that they are representative.

A cylindrical reservoir (circular in the plane of the domain) is used as this is the simplest possible; a cylindrical reservoir also allows for an incremental build-up of complexity starting from similar analytical elastic solutions mentioned above (e.g. Verruijt 1996 or Mogi 1958). Use of this geometry will be shown to lead to a number of useful conclusions about the underlying phenomena. As the resulting deformations for different reservoir geometries can be thought of as spatial convolutions of results presented here, these conclusions will also be applicable to more complex reservoir shapes. All results shown here are for reservoirs with a radius of 100 m at a depth of 4000 m as this depth and reservoir thickness is similar to the ones for the Netherlands gas fields (see Table 7.1 in NAM 2010).

A horizontal salt layer is included in all analyses and extends to the model edges. As this is the cap rock for the reservoir, (its low permeability means that it acts as a seal) in the majority of the analyses this is placed immediately over the top of the cylindrical reservoir. Salt layer thicknesses of 100, 200, 400, 800 and 1600 m are used so as to observe the effect of a varying layer thickness on the resulting deformation pattern and the time-dependence of subsidence observed at the surface. The effect of including an elastic layer of varying thickness between the top of the reservoir and the bottom of the rocksalt is also investigated as some gas fields in the Netherlands seem to be overlain by a relatively impermeable claystone layer (see e.g. NAM 2013).

Gas production from the reservoir material layer induces a pore pressure decrease inside it, which is assumed to be maintained after production as the reservoir is effectively sealed from its surroundings. This reservoir pore pressure decrease is modelled as an externally applied mean compressive stress of 1 MPa (with no shear stress) acting throughout the whole volume of the isotropic and elastic cylindrical reservoir. The motivation behind applying this mean stress increase in the reservoir material is that it is the effective stress (i.e. the total stress minus the pore fluid pressure) that is assumed to be carried by the solid material skeleton, and so responsible for causing deformation. As the total stress is constant, any pore pressure decrease due to compaction will lead to effective stress increases, which are directly linked to strains through the reservoir elastic moduli. The applied stress value of 1 MPa was chosen arbitrarily but as the stress and displacement magnitudes are proportional to the applied stress value (the problem is linear) the trends and mechanisms discussed here will be equally valid for any magnitude for the forcing. It should also be noted that in reality pore pressure is continuously depleted while the reservoir produces. However, here the focus remains on understanding the response to a step increase in reservoir compressive stress. This is because the response to a continuous decrease of pressure can be represented as a suitable time convolution of the step response.

As the mechanical equilibrium equations are linear and superposition of solutions applies, all models shown here only consider stress perturbations on top of the initial stresses that are in equilibrium with gravity forces. For tectonically inactive regions (such as the Netherlands—the motivation of this study), shear stresses in the rocksalt will have decayed to zero and so the initial stress state in equilibrium with gravity forces will produce no displacements. Deformations due to the stress perturbations applied are therefore the only ones relevant; initial stresses will not affect production-induced displacements. Gravity forces will also not significantly affect the time-dependent part of the flow as geometry changes in the Finite Element solution are very small. The above treatment of gravity forces thus neglects the buoyancy of the salt layer that can lead to diapirism. This is done on purpose as it is thought that in many situations the integrity of the rock overlaying the salt inhibits buoyancy-driven salt motion.

The material properties used for the analyses performed here are given in Table 1. These are only given here for completeness; it was found that results for different salt viscosities or elastic modulus magnitudes (but same elastic modulus distribution) can be unified if the correct non-dimensional quantity is plotted (time divided by Maxwell time or displacement divided by vertical ground displacement at the point $x = 0$, $y = 0$, a quantity that is inversely proportional to the Young's modulus of the materials in the domain). All analyses are performed with the same values of the elastic moduli

Table 1. The material properties used in the simulations. Note that the time can be non-dimensionalized by rocksalt Maxwell time and the time-dependent subsidence by the maximum elastic subsidence so that the response to different values of shear modulus or rocksalt viscosity can be unified. Therefore, the exact values for material properties used in the simulations do not influence results presented.

Shear modulus for all materials	2 GPa
Poisson ratio for all materials	0.25
Shear viscosity of salt layer	10^{18} Pa s
Bulk viscosity of salt layer	Infinite

and Poisson ratio throughout the whole of the domain. This is an over-simplification but allows for the significant effect of stiffness layering to be treated separately (part of a subsequent study). The solution at zero time is that of a fully elastic mesh therefore, which can be rationalized in a way similar to Verruijt (1996).

Spiers *et al.* (1990), van Keken *et al.* (1993), Urai *et al.* (2008) and Carter *et al.* (1993) among others, describe the behaviour of rocksalt in detail. In short, salt behaviour strongly depends on temperature, its grain size, its composition, water content and impurities content, and the shear stress or strain rate that is applied to it. For the Netherlands gas fields that motivate this study, the temperature is approximately 100 °C (e.g. Breunese *et al.* 2003), initial shear stresses inside the rocksalt are assumed to be zero (fully relaxed) and the grain size is expected to be between 3 and 20 mm (Breunese *et al.* 2003; NAM 2013). A pressure decrease in the reservoir of 0.5 MPa yr^{-1} can be assumed typical based on the data from the Groningen field given in NAM (2013). Approximately a third of that will be seen in Section 5.1 to be transferred to the salt layer as shear stress. The magnitude of these time-varying shear stresses will be relaxed by salt flow. Therefore, the shear stresses inside the salt layer due to gas extraction can be estimated to be of a maximum value of 10 MPa, assuming full reservoir depletion and no relaxation, with most probable a value that is even less than half of that, that is, of the order of a few MPa at any given time. It should be noted also that these values are upper estimates corresponding to locations in close proximity to the reservoir. Comparing these estimates of stress, strain rate, temperature and grain size, with a deformation mechanism map for rocksalt (e.g. Spiers *et al.* 1990; Spiers & Carter 1998; Urai & Spiers 2007), indicates that under these conditions salt flow falls near the transition between dislocation creep and pressure solution creep. For the smaller grain sizes and low shear stresses, a linear rheological model is most relevant (eq. 1). For higher stresses and large grain sizes, a non-linear rocksalt flow will take over, the full effect of this will be investigated in subsequent studies.

Our knowledge of the salt flow law relies mostly on few well-designed laboratory experiments that have been conducted at very low strain rates or stresses, and so are difficult to conduct. The reader should however note that another source of information can be the analysis of field-scale problems where rocksalt flow is relevant. Breunese *et al.* (2003) have commented on the applicability of certain rocksalt flow laws based on how well models using them fit the evolution of subsidence above a solution-mined rocksalt cavity. Li *et al.* (2012) have studied the gravitational sinking of inclusion of different density (stringers) within rocksalt to come to the conclusion that rocksalt viscosity needs to be non-linear over geological time scales. Our problem however involves deformation over different timescales over which linear salt creep seems equally relevant on the basis of experimental observations.

It should be noted that a linear salt flow law has been also used in past modelling analyses of Netherlands rocksalt bodies (e.g. Orlic & Wassing 2013). For grain sizes between 3 and 20 mm at 100 °C, the linear rocksalt creep equation given in Spiers *et al.* (1990) gives an absolute range of possible Maxwell times between 0.1 and 100 years for the Dutch gas fields respectively. Neither the higher nor the lower value are likely, but there remains a large uncertainty in the salt Maxwell time, a parameter that, as will be discussed below, controls the rate at which time-dependent subsidence will evolve. It should also be noted that at larger grain sizes power law creep will become dominant, itself reducing the response time (Maxwell time) for a rocksalt material element.

Further note that although we use linear rheologies in the models presented here, the interpretation of this approach can vary. First, the viscosity can be stress-independent as a result of diffusion creep. Second, linear flow can be an approximation of power law creep. This approximation may involve a linearization procedure as is sometimes used in mantle convection studies (after Christensen 1984). An alternative approximation of power law creep assumes that stresses and temperatures vary slowly, that is, a linear viscosity can be thought of as a local approximation to a non-linear flow. On longer time scales, stresses and temperatures likely will change, so our results cannot be extrapolated to geological time scales, especially if a non-linear rocksalt rheology is more relevant. Finally a linear salt flow model with a reduced elastic modulus has also been used to model rocksalt transient creep (e.g. Prij 1991). The full effect of a non-linear steady-state flow law and transient creep will form part of subsequent studies.

5 RESULTS FOR THE REFERENCE MODEL (400 m THICK ROCKSALT)

5.1 The elastic solution (common to all models)

The deformation of the model reservoir can be separated into an elastic part, which occurs immediately after the application of the reservoir pore pressure decrease (i.e. the mean compressive stress increase), and a time-dependent part, which is driven by stress relaxation and flow inside the viscoelastic rocksalt layer. The elastic (immediate) deformation is the same for all models presented here. This is because all layers have the same elastic properties (the rocksalt is modelled as a Maxwell material that has an additional viscous element). It is just the thickness and location of the rocksalt layer that distinguishes between the different models discussed here.

The elastic displacement field for a reservoir mean compressive stress increase of 1 MPa is plotted in Fig. 2. Only half the domain is plotted as the displacement mechanism is fully symmetric about a vertical line passing through the centre of the reservoir. The displacement is towards the reservoir (located at $x = 0$ and $y = -4000$ m) from all directions, but there is more movement from the top. This is due to the presence of the top free surface. Such a displacement field is very similar to the analytical solution given by Verruijt (1996), which is however for a slightly different boundary condition at the reservoir.

The horizontal and vertical elastic surface displacements are plotted in Fig. 3. It shows that the subsidence trough initially extends to much larger widths than the lateral extent of the reservoir (100 m here). This is typical of such problems; for example in the context of the similar problem of tunnelling through soil, Rankin (1988) shows

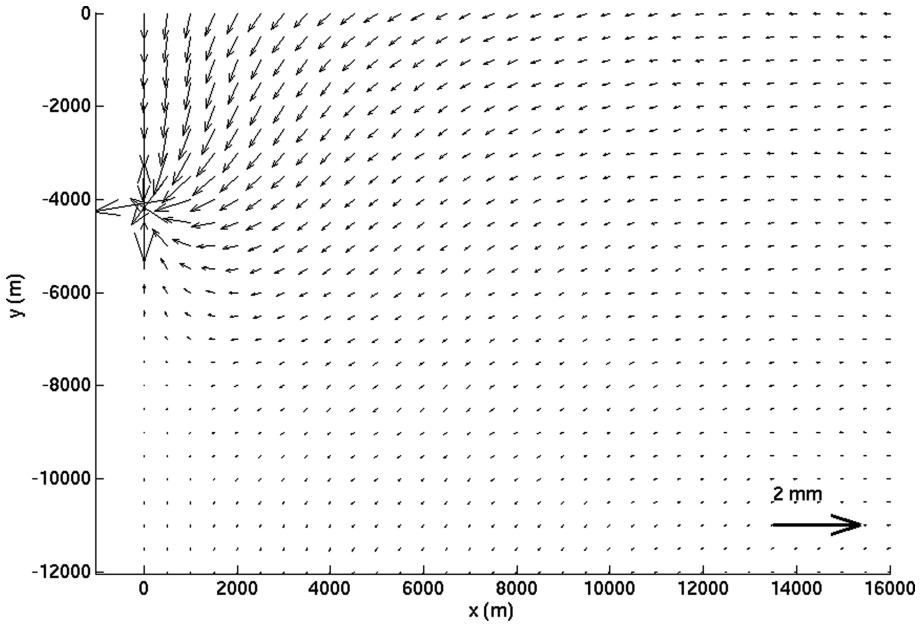

Figure 2. The elastic displacement field for half of the mesh. This is common to all models.

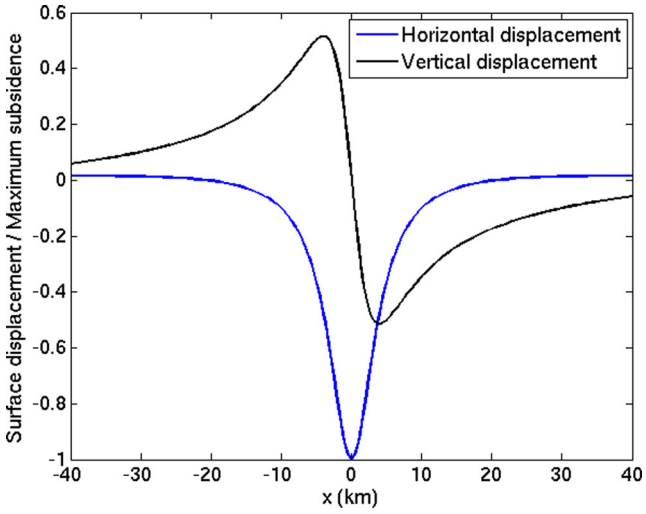

Figure 3. The horizontal and vertical elastic surface displacements (i.e. at $t = 0$) plotted against distance from the reservoir centreline.

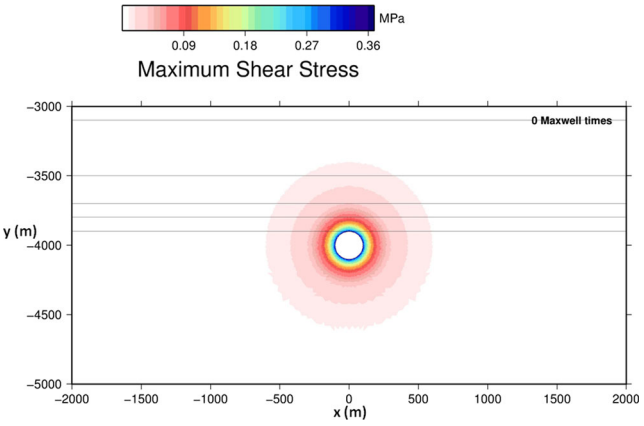

Figure 4. A contour plot of the maximum shear stress for all models immediately after loading ($t = 0$). The bottom faint horizontal line marks the bottom level of the salt layer in the case where this is in contact with the top of the reservoir, and the other faint lines mark the top of the salt layer when this is 100, 200, 400 and 800 m thick, respectively.

that the width of the surface subsidence trough can be well correlated to the cavity's (tunnel) depth. There are significant ground movements at distances of up to eight times the reservoir depth meaning that solutions for meshes that extend to much smaller widths cannot be accurate. Horizontal surface displacement magnitudes are of the same order as vertical ones and are towards the reservoir location. It should be noted that subsidence magnitudes are for a uniform distribution of elastic parameters through the domain. Normalizing by maximum elastic subsidence unifies the behaviour of simulations conducted with different values for the material elastic modulus.

In problems where the cavity considered is a tunnel inside shallow sedimentary layers there is a large amount of field evidence to suggest that the elastic vertical displacements should follow a Gaussian curve (see Peck 1969; Rankin 1988 for example). Puzrin *et al.* (2012) highlighted that elastic analyses similar to the above often fail to reproduce the empirically expected Gaussian curve. Bym *et al.* (2013) further noted that such a Gaussian curve could be reproduced by a Discrete Element model of the ground, that is, a model that allows for more freedom of deformation between material points. It is unknown whether such Gaussian-type vertical displacement should also be expected for the deeper cavity collapse problems relevant to the reservoir pressure depletion problem. Active surface displacement data collection campaigns should be able to shed light into this topic. These would help assess whether isotropic elastic analyses similar to the one conducted here also produce wider subsidence troughs than ones observed in the field for deep reservoir-induced deformations (a 3-D problem), as they do for shallow tunnelling-induced surface subsidence (a 2-D problem).

Fig. 4 shows a contour plot of the maximum shear stress. The shear stress magnitudes are largest at the edge of the reservoir and decrease proportionally to the square of the distance from it. This is an important observation as viscous strain rates (proportional to the maximum shear stress—see eq. 1) will be largest at the point where the reservoir touches the rocksalt layer. The magnitude of the maximum shear stress is 0.38 MPa, or 38 per cent of the applied reservoir pressure decrease for the situation considered here. This

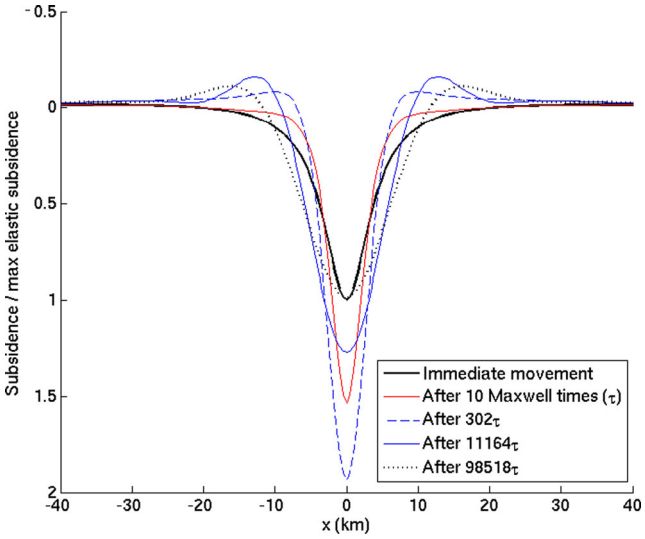

Figure 5. A plot of the spatial distribution of normalized vertical surface subsidence for the case of a salt layer 400 m thick plotted at a number of different time instances.

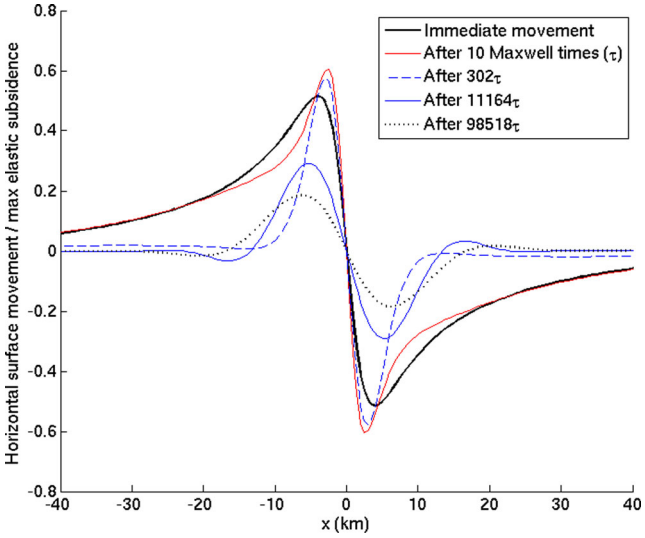

Figure 6. A plot of the spatial distribution of normalized horizontal surface displacement for the case of a salt layer 400 m thick plotted at a number of different time instances.

observation is significant as it can help constrain the maximum expected shear stresses (useful for the discussion of rocksalt flow laws, see Section 4 above).

5.2 Evolution of surface displacements

Figs 5 and 6 plot the vertical and horizontal ground surface movements as a function of horizontal distance from the centreline of the reservoir (located at $x = 0$) at a number of different time instants. Time is non-dimensionalized by the Maxwell time for the viscous layer and displacements by the maximum elastic subsidence as this unifies the behaviour for models of different elastic moduli and salt viscosity.

As can be seen in Fig. 5, the subsidence trough initially becomes deeper and narrower, then develops some uplift and finally becomes shallower as the region of uplift moves laterally away from the reservoir's centre-line. Fig. 6 shows that the maximum horizontal movement that is expected at the ground surface is of the same order of magnitude as the vertical subsidence. This means that it should be in principle possible to measure such horizontal movements in the field, which might in turn be able to constrain the underlying phenomena in the ground. It should be noted however that the maximum subsidence takes approximately 75 Maxwell times to develop, so velocities of salt-flow driven surface deformation might be very small if salt Maxwell times are large.

Fig. 7 shows the temporal evolution of vertical subsidence for a point at $x = 0$. This is the location where ground displacements are at a maximum and so most easy to measure in the field. From Fig. 7, it is apparent that the deformation does not stop even after very large times. However, it seems to tend asymptotically towards a final value. Fig. 7 also shows that the initial deepening of the trough is relatively fast, followed by a much slower shallowing. The shift from deepening to shallowing can be associated with a switch from one dominant mechanism (rocksalt shear stress relaxation, which we call 'the shear stress flow mechanism') to another (flow within the confined conduit of the rocksalt layer, which we call 'the pressure flow mechanism'). This will be further discussed in Section 5.3 below. It is important to keep in mind that our model results are obtained based on a linear viscosity. This is an approximation of the (more complex) real mechanical properties of rocksalt; see Section 4 above.

5.3 A detailed look at the resultant flow field

Fig. 8 shows the velocity field at 0.1 Maxwell times after the mean stress increase application. As can be seen the initial velocities are such that the reservoir sinks and there is movement of the salt towards it. The movement of the rocksalt induces a similar movement at the top of the elastic layer just below it, which in turn leads to the development of a circulation pattern there so as to ensure material continuity. At the top of the salt layer, the movements are much smaller (almost negligible) as the shear stresses there are smaller and are further constrained by the relatively thick (and relatively stiff) top elastic layer.

Fig. 8 also plots a contour of the difference between the horizontal and vertical stresses ($\sigma_{xx} - \sigma_{yy}$). This is done to aid interpretation; $\sigma_{xx} - \sigma_{yy}$ is the quantity that appears in the constitutive equations for the strain rates in the x (horizontal) and y (vertical) directions (see eq. 1). Note though that the strain rates have two components, one due to the viscous flow (only present in the rocksalt layer) and one due to elastic stress redistribution. As can be observed the stress difference ($\sigma_{xx} - \sigma_{yy}$) is negative and of largest magnitude just above the reservoir. This means that there will be negative strain rates (contraction) in the x direction and positive (extension) in the y direction. This explains why the bottom of the rocksalt moves horizontally towards the $x = 0$ line (which is constrained due to symmetry to have no horizontal displacement). The extension in the y direction is then accommodated by a downwards movement towards the reservoir. In order to satisfy material compatibility, the reservoir moves downwards and a circulation pattern in the bottom elastic layer develops. The top of the rocksalt layer, located in an area where there is little shear stress is not perturbed from its elastic equilibrium as fast and so there, the rates of deformation are very small in comparison to the areas of high shear stresses. The movements of the ground surface at this stage are also small in comparison, however, a slight deepening and narrowing of the vertical surface displacement curve is observed (see Fig. 5).

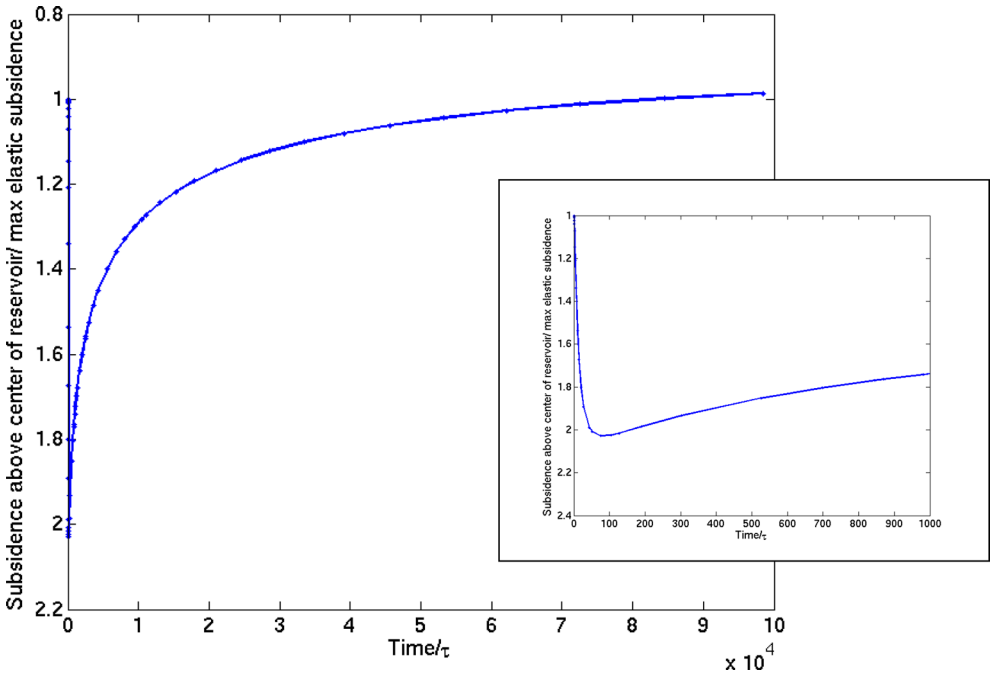

Figure 7. The normalized plot of subsidence versus time for the point immediately above the reservoir's centreline for the case of the 400 m thick viscous layer that is in contact with the top of the reservoir. Inset: a zoomed-in version of the same plot.

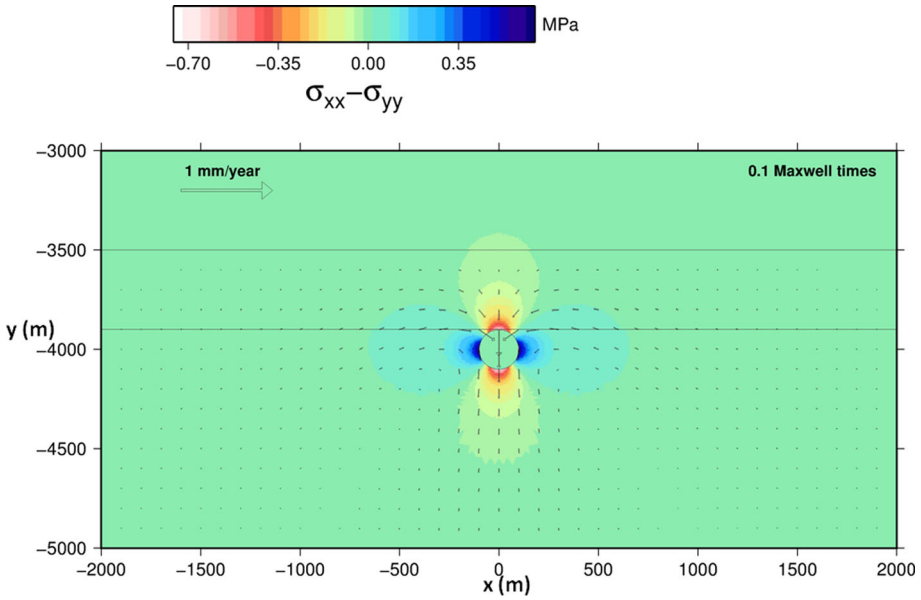

Figure 8. The velocity field and a contour plot of $\sigma_{xx} - \sigma_{yy}$ for the 400 m thick viscous layer that is in contact with the top of the reservoir at a time of 0.1 Maxwell times after the application of the model reservoir mean stress increase.

Fig. 9 shows the shear stress contours and velocity field at a time of 4.2 Maxwell times. When comparing to Fig. 4 one can note that there is significant stress relaxation inside the rocksalt layer. The velocity field is similar to that in Fig. 8 in that a circulation pattern is again observed inside the bottom layer. However, the velocities inside the top elastic layer are no longer negligible in comparison to the ones in the rocksalt layer. Note also that the scale for velocity is different in the two plots.

Fig. 10 plots the shear stress contours and velocity field for a time of 79.4 Maxwell times. Shear stresses within the viscous layer are almost fully relaxed and a change in the flow pattern is observed. Flow is now mostly concentrated inside the salt layer with salt being drawn into the region above the reservoir. This causes the ground surface over the reservoir centre to experience some upwards movement. The upwards movement of the surface can also be explained by considering the top elastic layer as a slab or beam that is initially flexed downwards fully by the contracting reservoir. As the shear stresses in the rocksalt layer relax the top slab gets partially uncoupled from the deformation source region and so flexes upwards.

Focusing now on the viscous layer, the shear stresses inside it have almost fully relaxed. Fig. 11 plots the mean stress field at the same point in time, again with the material velocity field. Note that the contour levels plotted have been limited to between −2 and 2 kPa,

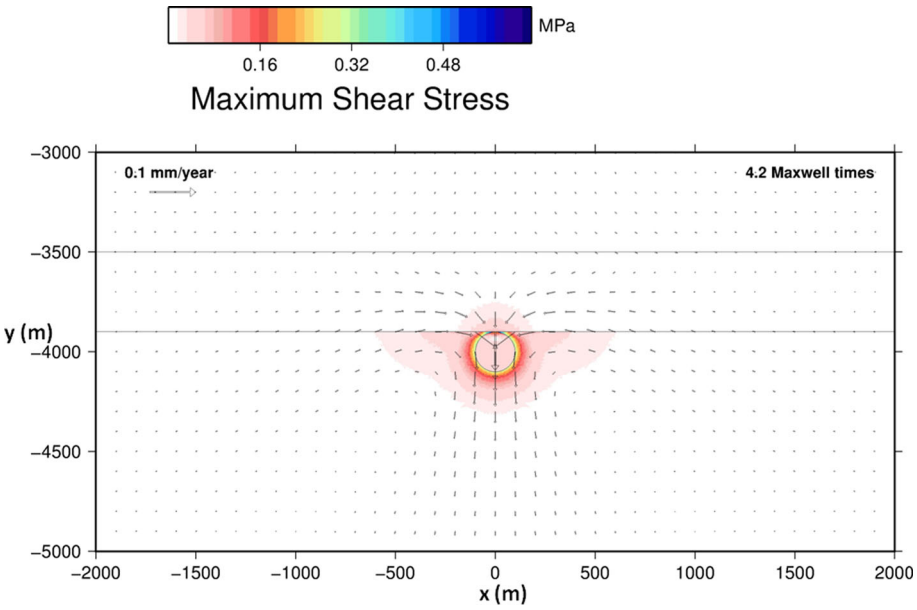

Figure 9. The velocity field and maximum shear stress contour plot for the 400 m thick viscous layer that is in contact with the top of the reservoir at a time of 4.2 Maxwell times after the application of the model reservoir mean stress increase.

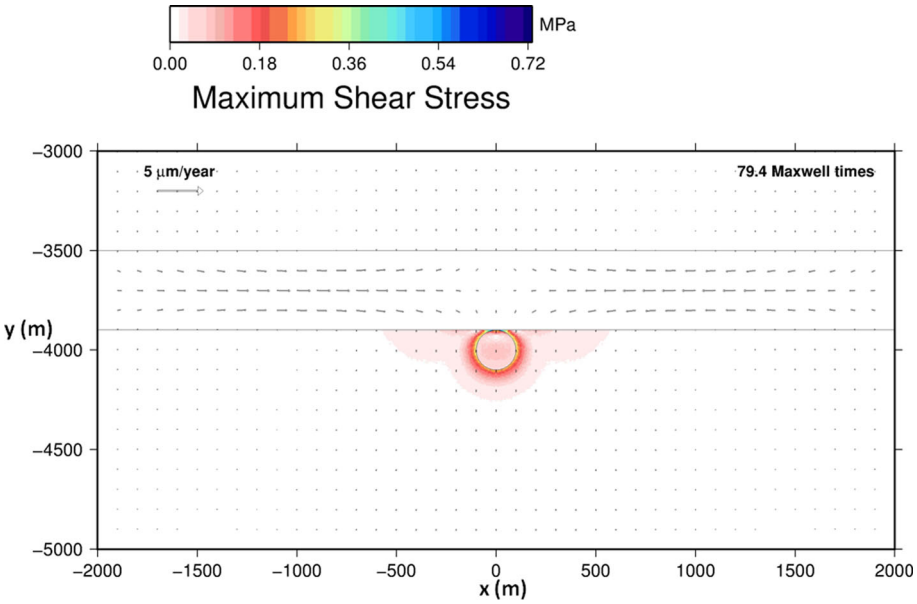

Figure 10. The velocity field and maximum shear stress contour plot for the 400 m thick viscous layer that is in contact with the top of the reservoir at a time of 79.4 Maxwell times after the application of the model reservoir mean stress increase.

that is, that any levels above or below that have been assigned to white or blue respectively. As can be seen the flow in the salt layer is driven by the differences in the mean stresses and is consistent with flow within a confined conduit that extends the whole width of the viscous layer (see also Figs 10 and 12). At its edges there is very little material movement. A region of compression (higher mean stress relative to the surroundings) at the point of x equal to 2.4 km acts as a driver of flow, with flow occurring in two directions away from the compression region. This flow pattern allows for the mean stress within the salt layer to equilibrate at zero, at ever-decreasing rates. The picture observed at larger Maxwell times is very similar to that of Fig. 11, the main difference being that the region of compression migrates to higher distances away from the reservoir (towards the far field) and its mean stress decreases in magnitude. Fig. 12 shows a plot of the velocity distribution inside the viscous layer at a time of 79.4 Maxwell times. It further confirms the mechanism of flow within a confined conduit (which we call here the 'pressure flow mechanism').

6 EFFECT OF VARYING THE ROCKSALT LAYER THICKNESS

A number of simulations with varying salt thicknesses are presented here. In all cases shown in this section, the bottom of the salt layer is in contact with the top-most point of the model reservoir. The only thing that varies is the location of the top of the salt layer (i.e. the layer thickness). Fig. 13 plots the evolution of the maximum

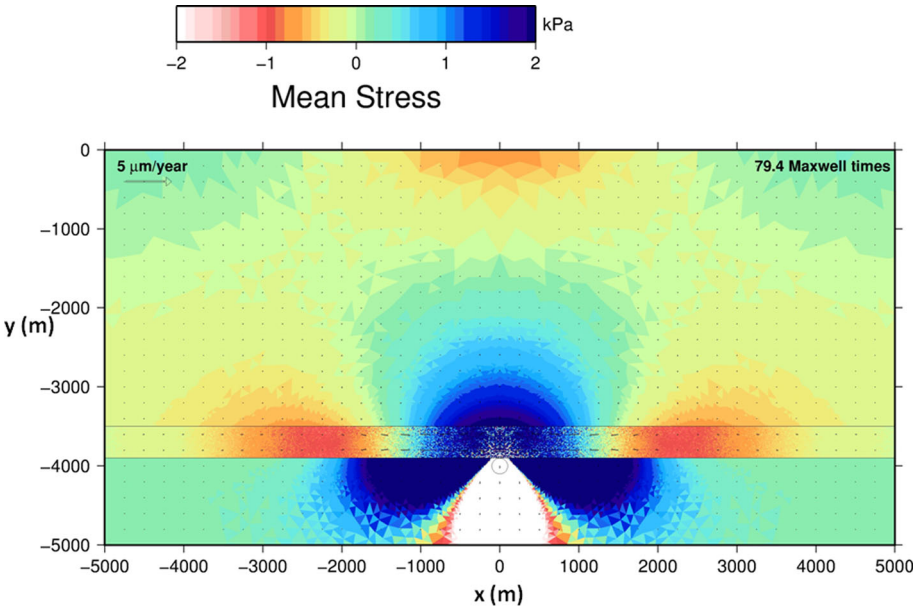

Figure 11. The velocity field and mean stress (i.e. $(\sigma_{xx} + \sigma_{yy})/2$) contour plot for the 400 m thick viscous layer that is in contact with the top of the reservoir at a time of 79.4 Maxwell times after the application of the model reservoir mean stress increase.

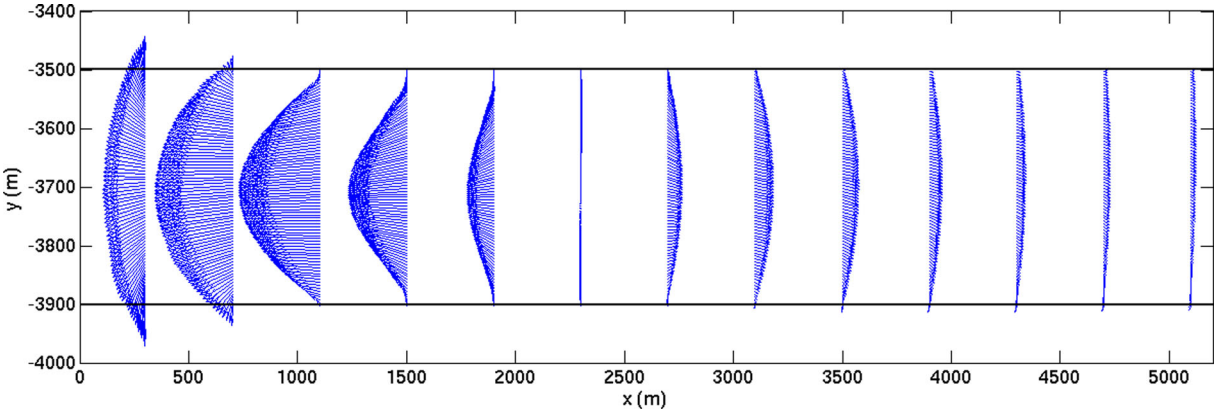

Figure 12. The velocity field inside the 400 m viscous rocksalt layer at a time of 79.4 Maxwell times after the application of the model reservoir mean stress increase.

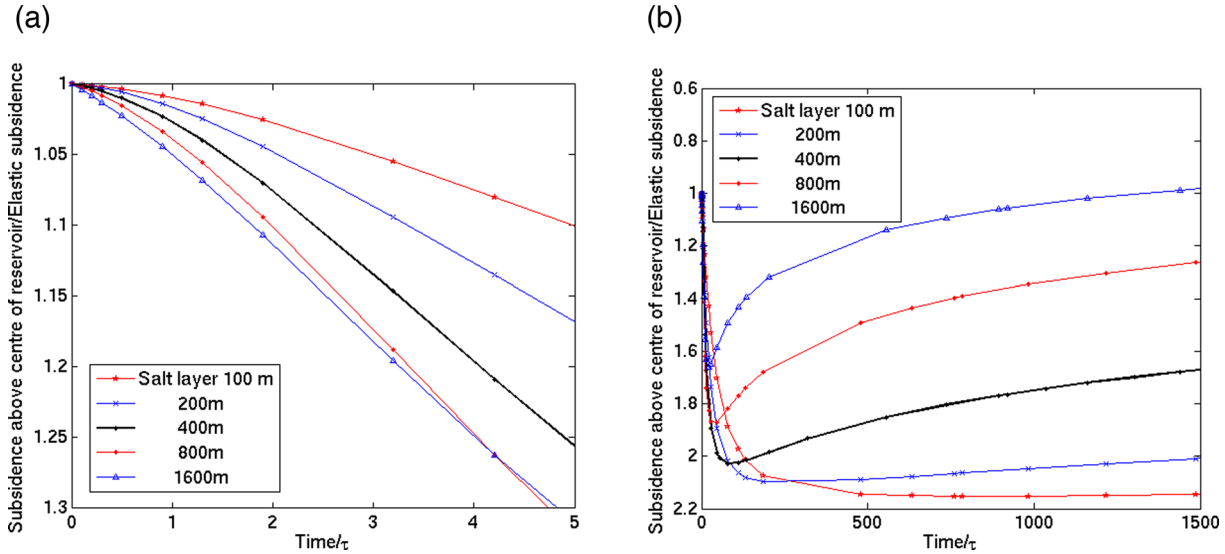

Figure 13. The normalized plot of subsidence versus time for the point at the ground surface immediately above the reservoir centreline. Results shown are for simulations where the rocksalt layer is in contact with the top of the reservoir but is of varying thickness: (a) zoomed-in version; (b) full version.

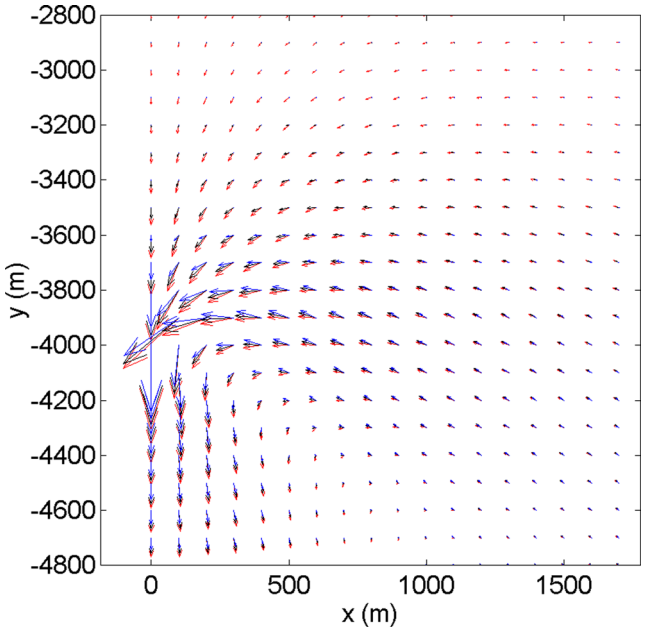

Figure 14. A plot of the initial material velocity fields for the case of 400 m (blue), 800 m (black) and 1600 m (red) rocksalt region whose bottom is in contact with the top of the model reservoir.

vertical displacement of the surface (the surface point immediately above the reservoir) with time. Note that both the x and y axes of the plot have been non-dimensionalized. Also note the elastic subsidence of that point, used to non-dimensionalize the y axis, is the same (within numerical error) for all simulations presented in this paper. Any scatter in its value is negligible and can be attributed to discretization differences.

Similar to the simulation for the 400 m thick salt layer all results show that the subsidence trough deepens and becomes narrower initially. Fig. 13(a) shows that the initial rate of deepening increases with increasing salt layer thickness. Fig. 14 shows the material velocity fields for salt layer thicknesses of 400 m (blue), 800 m (black) and 1600 m (red). As can be seen the top elastic layer acts so as to restrain the material movement; most of the movement occurs below this. This top layer can be thought of as a slab. The thicker the top layer the more stiff it is, and so the less it deflects downwards for a given displacement imposed by the viscous stress redistribution. Therefore the rate of initial downwards movement is largest for the thinnest top elastic layer (thickest salt layer) and decreases with decreasing salt layer thickness. There is also a secondary effect present—the thicker the salt layer, the larger the region inside which the shear stresses need to relax, and so the larger the region for which viscous strain rates exist (displacement rates are the spatial integrals of strain rates and so these are larger for the thicker salt layers). However, this effect is not dominant as the shear stresses decay rapidly with distance from the reservoir (see Fig. 4).

It should also be noted that all curves in Fig. 13(b) exhibit a minimum after which the free surface immediately above the reservoir starts moving upwards. This turnaround point occurs faster for the thicker salt layers. This can be explained by considering the two mechanisms described in Section 5.3 above, namely the stress relaxation mechanism (‘the shear stress flow mechanism’), dominant initially, and the confined conduit flow mechanism (‘the pressure flow mechanism’), dominant at larger times. The thicker the salt layer the wider the conduit and so, the flow is subject to less resistance by the conduit’s sides. Also, as discussed above, the wider

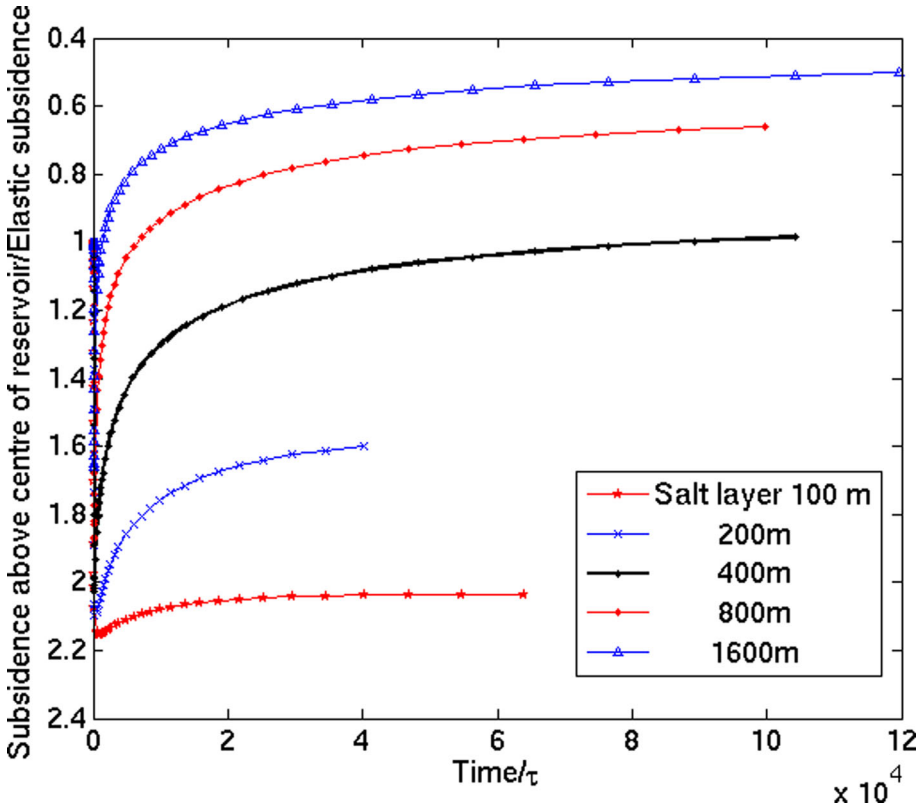

Figure 15. The full extent of the normalized plot of vertical subsidence versus time for the point at the ground surface immediately above the reservoir centreline. Results shown are for simulations where the rocksalt layer is in contact with the top of the reservoir but is of varying thickness.

the conduit (salt layer) the thinner and less stiff the top elastic layer (slab). Therefore, as a result of the flow inside the conduit, the top surface is subjected to more upwards movement for the thicker salt layer. This is confirmed by Fig. 15, which shows that the final vertical surface subsidence above the reservoir is larger for the 100 m thick salt layer and smallest for the thickest.

7 THE INITIAL TIME-DEPENDENCE OF VERTICAL SURFACE SUBSIDENCE

An element of the viscoelastic material used here is characterized by its Maxwell time constant (τ), that is, the ratio of its viscosity to its shear modulus. The stress inside an element of such a material will follow an exponential time decay if a sudden strain is applied to it at $t = 0$ of the form $e^{-t/\tau}$. As also mentioned above the Maxwell time of the salt layer can be used to normalize time and unify the response of simulations that differ only in salt viscosity. This proportionality of the time-response of course can only be expected to hold for the linear viscoelastic material models used here; for non-linear salt models the dependence on a characteristic time parameter similar to Maxwell time will also be non-linear.

It should be stressed however that the response at the surface is not identical to the response of a material element. The response discussed here is complex, each viscoelastic material element is subjected to different conditions, and the response of surface displacements depends on the exact combination of geometry and conditions inside all the relevant material elements. This is the reason why the response seen in Figs 7, 13 or 15 is so different to that of single material elements.

The initial parts of the maximum vertical subsidence versus time plots (Fig. 16) seem however to follow a curve that to some approximation can be fit by an exponential decay. Given that a fully empirical exponential-like time decay has been suggested as fitting relatively well the limited data available from field studies of reservoir-induced subsidence (e.g. NAM 2013), it is of merit to investigate this point further. Fig. 16 plots the initial data for subsidence versus time overlain by least-squares exponential decay fits

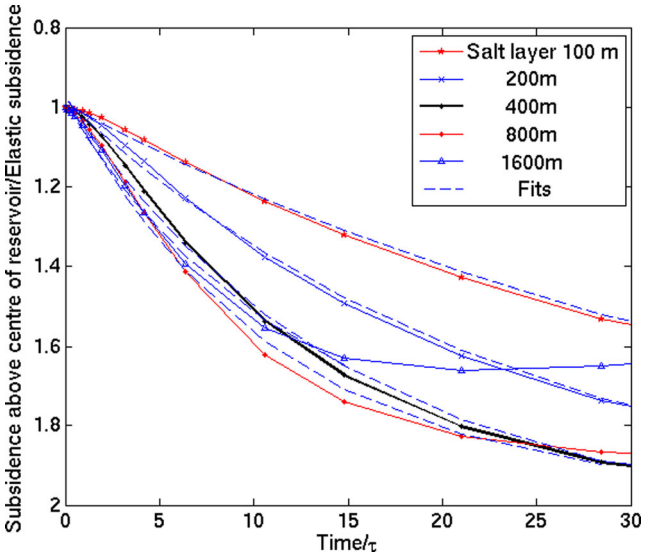

Figure 16. The initial part of the normalized subsidence versus time curve for the situation where the rocksalt layer and reservoir are in contact. Exponential decay fits to the data have been also plotted.

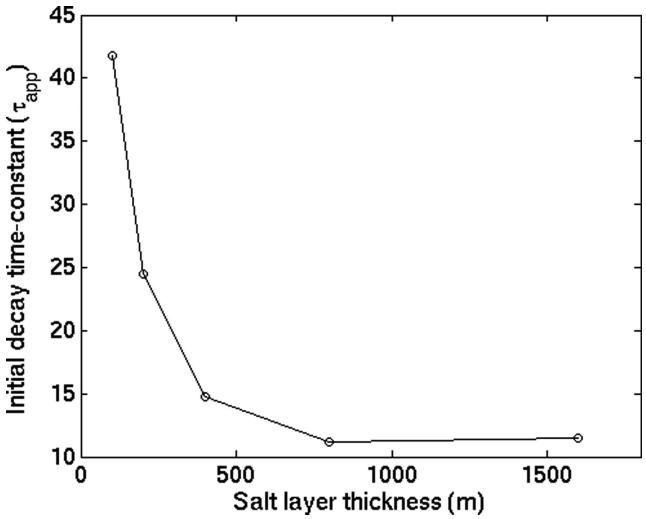

Figure 17. The exponential decay times versus salt layer thickness as obtained by the fits to the initial subsidence versus time data shown in Fig. 16.

to the data. This fit was performed using MATLAB. As can be observed this empirical fit is relatively good, but not perfect.

Nevertheless, as available field data might only cover the initial part of the deformation, this exponential fit might be useful as a simple way of describing the initial variation of maximum subsidence. The resultant best-fit time decay constants are plotted in Fig. 17 as a function of salt layer thickness. Even though the decay time observed is proportional to the salt layer's Maxwell time (τ) the geometry of the problem is seen to be a very important controlling factor on its exact value. The thinnest salt layers take longer to respond to the pore pressure perturbation at the reservoir, while it seems that above a certain viscous layer thickness the speed at which deformation occurs is no longer controlled by the thickness of the salt layer. It should be further noted that the decay time for the whole geomechanical system is never equal to the decay time for a material element.

Fig. 18 shows the vertical subsidence versus normalized time for a point at the ground surface 4 km away from the centre-line of the reservoir. This plot confirms that any time-decay initially relevant for the point immediately above the reservoir is no longer applicable for this other points at the ground surface. It further indicates that in order to fully comprehend the deformation pattern, surface subsidence needs to be sampled at a large number of points. It finally hints to the sensitivity of the time-dependence of subsidence on its exact sampling location, and so, highlights the danger of using a simple empirically derived exponential decay fit on real data.

8 EFFECT OF INCLUDING AN ELASTIC LAYER BETWEEN THE RESERVOIR AND THE SALT LAYER SEAL

In some of the Netherlands gas fields, the reservoir and the rocksalt layer are separated by a claystone layer. This is the motivation behind including an elastic layer between the top of the reservoir and the rocksalt layer, that is, offsetting the viscoelastic layer upwards by a varying distance while keeping the reservoir location the same. Fig. 19 shows the normalized maximum subsidence versus time curves for a number of such simulations. The plots of Fig. 19 can be separated in two subsets. In the first subset, the salt layer is 400 m thick but is offset upwards by a distance of 50, 100 or 200 m from the top of the reservoir. As can be observed the effect of this

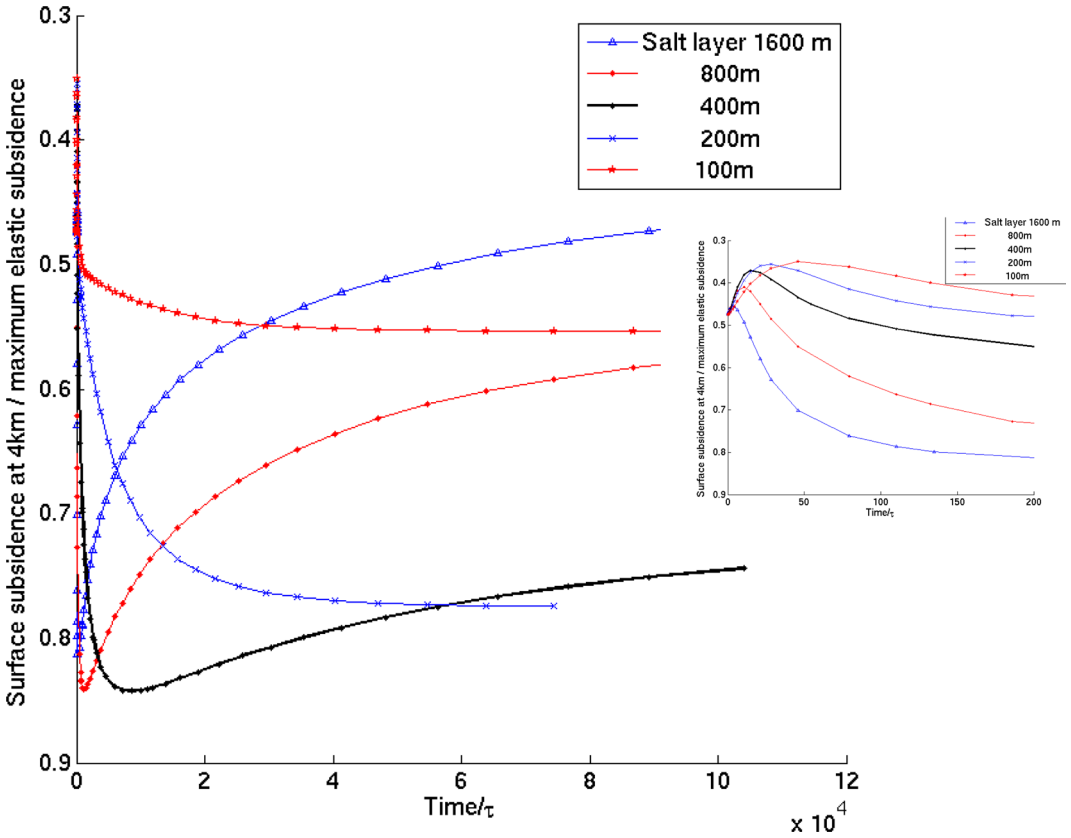

Figure 18. The evolution of surface subsidence at a surface point 4 km away from the centreline of the reservoir. Results shown are for simulations where the rocksalt layer is in contact with the top of the reservoir but is of varying thickness. Inset: a zoomed-in version of the same plot.

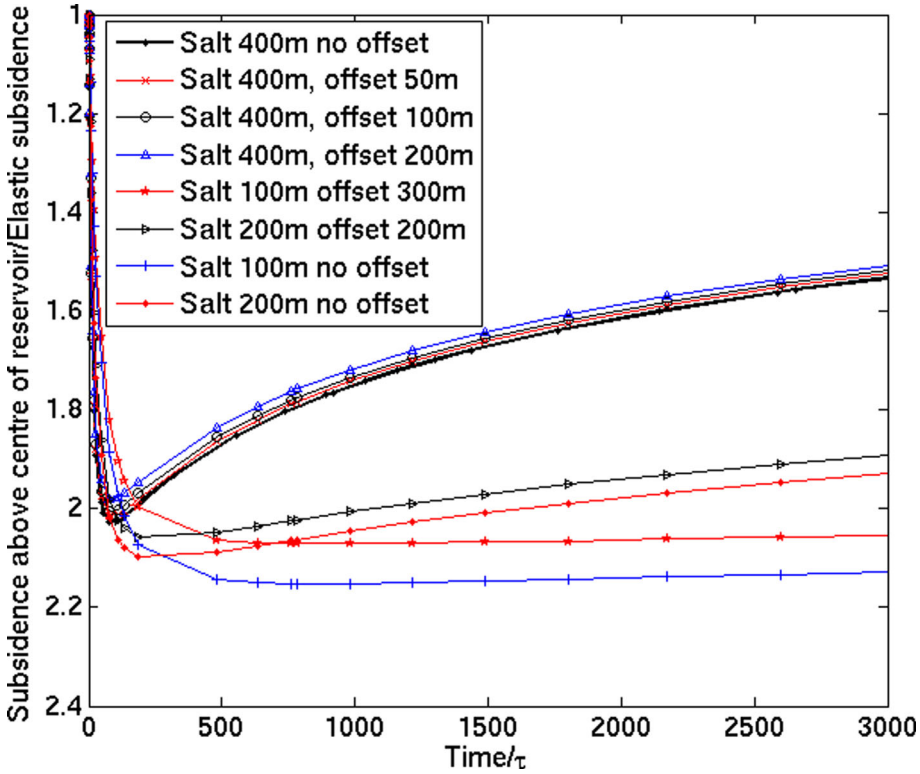

Figure 19. The normalized plot of vertical subsidence versus time for the point at the ground surface immediately above the reservoir centreline. Results shown are for some simulations where the salt is in contact with the reservoir and others where the rocksalt layer is offset by some distance from the top of the reservoir.

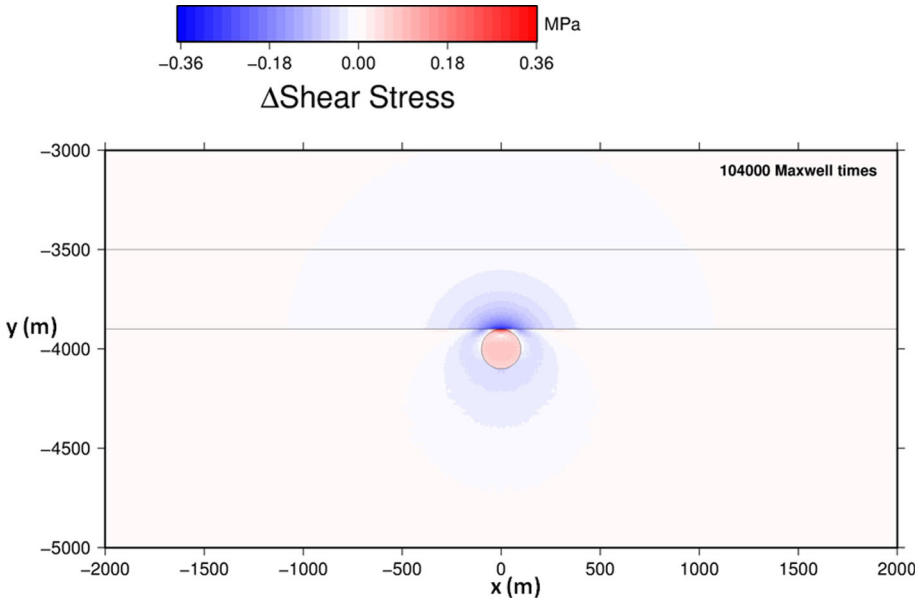

Figure 20. The difference in the maximum shear stress magnitudes between a point that is close to the end of the time-dependent deformation and a point immediately after the application of the forcing (the elastic stresses). A positive value in the plot therefore indicates an increase in the maximum shear stress magnitude due to linear rocksalt flow.

on the maximum subsidence versus time plot is very small. The differences can be attributed to the smaller shear stresses that need to be dissipated if the salt layer is moved away from the reservoir, and also to the slightly thinner top elastic slab that needs to be flexed upwards.

In the second subset of simulations, the thickness of the top elastic slab is kept constant (3500 m) and so both the salt layer thickness and the offset are simultaneously changed to reflect that. The results show that the thickness of the top slab does not affect significantly the resultant time-dependence of subsidence. The results for same salt layer thickness but different offset however display similar time-dependence, further confirming the argument of a flow-through-a-conduit-like structure as discussed above. It should also be noted that the location of the top of the salt layer (kept the same in this subset of simulations) does not seem to affect the level at which the model equilibrates at large times so much.

9 A NOTE ON STRESS REDISTRIBUTION

Figs 4, 9 and 10 show that the shear stress distribution changes with time. Flow in the rocksalt layer leads to shear stresses retention in the elastic layer just below it as the shear stresses inside the salt relax. The shear stresses above the salt layer are reduced. Fig. 20 below is a contour plot of the maximum shear stress magnitude at a time close to the end of the time-dependent deformation minus the maximum shear stress magnitude at time zero, (i.e. the elastic solution as shown in Fig. 4). A positive value means an increase in the maximum shear stress magnitude with time. Note however that the direction along which the maximum shear stress acts might have changed. This plot therefore can help highlight regions which might be pushed closer to failure because of rocksalt flow, assuming that maximum shear stress is a proxy for failure. Note that these regions are inside the reservoir.

However, when trying to identify regions prone to inelastic material response, the shear stress plots of Figs 4, 9 and 10 are the most important, as these show absolute changes in shear stress since the start of the reservoir depletion. Based on these figures a region that gets highly stressed due to production is the one immediately outside the model reservoir. As in many cases reservoirs are bounded by faults this observation could be significant. The time-dependence which is the focus of this study will also be relevant for induced seismicity. Readers should however keep in mind that this conclusion is based on the modelling assumptions made here, which have only considered linear rocksalt flow and idealized material response elsewhere as isotropic and elastic. The shape of the reservoir is very important too; our preliminary analysis of different reservoir shapes has shown that reservoir material for different reservoir shapes can also be sheared significantly.

10 CONCLUSIONS

The simulations presented here test the simplest possible geometry and material properties distribution with the aim of clarifying aspects of the time-dependent deformation above a model reservoir that is being depleted. A number of conclusions have been reached, which are as follows:

(1) The most important conclusion is that there is the potential for significant additional time-dependent surface subsidence due to shear-stress-induced flow and shear stress relaxation inside a rocksalt layer.

(2) Two mechanisms by which deformation evolves have been observed, each having a different timescale associated with it. The first and fastest (‘the shear stress flow mechanism’) is directly linked to shear stress relaxation at highly stressed rocksalt regions in the immediate vicinity of the reservoir. The second and slowest of the two (‘the pressure flow mechanism’) can be described as a mechanism driven by mean stress equilibration inside the rocksalt layer, leading to a closed conduit-type flow inside it.

(3) Apart from the rocksalt material viscosity, the rocksalt layer thickness seems to be the key factor in controlling the relative speed at which these two mechanisms develop with consequences on both the maximum subsidence and the final subsidence at large times.

(4) The thinner the salt layer the larger the maximum subsidence and the longer the time it takes for it to be reached.

(5) The thinner the salt layer the smaller the eventual recovery from maximum subsidence, that is, the smaller the post-maximum rebound.

(6) The initial part of the time versus vertical surface subsidence curve for the point immediately above the centreline of the reservoir is observed to broadly follow an exponential decay. This empirical initial decay time constant is severely affected by the geometry of the problem (larger for thinner salt layers). It is proportional to the rocksalt material Maxwell time (i.e. the quantity that characterizes the decay of stresses inside a material element that is stressed), but can be many times larger than that.

(7) The exact time-dependence of surface subsidence as induced by rocksalt flow is dependent on the location of the point for which surface displacement is shown. In order to fully understand the time-variation of surface displacements in the field, these need to be sampled at a number of points, over areas larger than the extent of the reservoir itself.

(8) There are significant production-induced horizontal displacements. The magnitudes of these are slightly smaller than in the case of the vertical displacements. Nevertheless, collection of both horizontal and vertical displacements from the field would be useful when comparing with numerical models similar to the ones presented here.

The stress redistribution around a producing reservoir has been touched upon too. It has been observed that

(1) There is a shear stress increase in the region around the model reservoir that occurs instantaneously upon the reservoir mean stress reduction that is associated with pore pressure decrease and hydrocarbon production. This might be significant as reservoirs are often bounded by faults.

(2) Flow inside the viscous salt layer might reduce some of these shear stresses around the reservoir but slightly increase the shear stresses inside the reservoir for the simple reservoir shape chosen here.

The above provide a framework for qualitatively describing the behaviour for the geometries tested here. Adding further levels of complexity to this model would allow for the behaviour to be rationalized one step at a time with the final aim of better understanding the factors responsible for the observed time-dependence of subsidence in the field. For example, elastic properties layering and layer non-horizontality have not been included in the model; these could have a significant additional effect on the observed deformations.

Finally, results presented here are also relevant for a number of other physical problems that involve viscoelastic material layers and underground sources of deformation. Possibly the most important conclusion is that surface displacement response cannot be fit with a simple exponential decay as obtained through a single material element. This realization can have far reaching consequences on topics as diverse as post-glacial tectonic rebound, post-seismic stress relaxation, or volcanism-induced ground movements.

ACKNOWLEDGEMENTS

We would like to acknowledge financial support from NAM. Helpful discussions with Drs Anthony Mossop and Rob van Eijs of NAM/Shell are gratefully acknowledged. We also thank Lukas van der Wiel and Theo van Zessen for computing support, Professor Janos Urai and an anonymous reviewer and the Associate Editor (Prof Jörg Renner) for constructive comments.

REFERENCES

Breunese, J.N., van Eijs, R.M.H.E, de Meer, S. & Kroon, I.C., 2003. Observation and prediction of the relation between salt creep and land subsidence in solution mining - The Barradeel case, in *Proceedings of the Solution Mining Research Institute Fall 2003 Conference,* Chester, United Kingdom.

Bym, T., Marketos, G., Burland, J.B. & O'Sullivan, C., 2013. Use of a two-dimensional discrete-element line-sink model to gain insight into tunnelling-induced deformations, *Géotechnique*, **63**(9), 791–795.

Carter, N.L., Horseman, S.T., Russel, J.E. & Handin, J., 1993. Rheology of rocksalt, *J. Struct. Geol.,* **15,** 1257–1271.

Christensen, U., 1984. Convection with pressure- and temperature-dependent non-Newtonian rheology, *Geophys. J. R. astr. Soc.,* **77,** 343–384.

Fokker, P.A. & Orlic, B., 2006. Semi-analytic modelling of subsidence, *Math. Geol.,* **38,** 565–589.

Fokker, P.A., Urai, J.L. & Steeneken, P.V., 1995. Production-induced convergence of solution mined caverns in magnesium salts and associated subsidence, in *Proceedings of the Fifth International Conference on Land Subsidence,* pp. 281–289, eds Barends, F.B.J., Brouwer, F.J.J. & Schröder, F.H., The Hague, The Netherlands.

Gambolati, G., Teatini, P. & Ferronato, M., 2006. Anthropogenic land subsidence, *Encyclopedia of Hydrological Sciences,* **13,** 158, doi:10.1002/0470848944.hsa164b.

Geertsma, J., 1973. A basic history of subsidence due to reservoir compaction: the homogeneous case, *Verhandelingen Koninklijk Nederlands Geologisch en Mijnbouwkundig Genootschap,* **28,** 43–62.

Geertsma, J. & van Opstal, G., 1973. A numerical technique for predicting subsidence above compacting reservoirs, based on the nucleus of strain concept, *Verhandelingen Koninklijk Nederlands Geologisch en Mijnbouwkundig Genootschap,* **28,** 63–78.

Gerya, T.V., 2010. *Introduction to Numerical Geodynamic Modelling,* Cambridge Univ. Press, pp. 260–261.

Govers, R. & Wortel, M.J.R., 1993. Initiation of asymmetric extension in continental lithosphere, *Tectonophysics,* **223,** 75–96.

Govers, R. & Wortel, M.J.R., 1999. Some remarks on the relation between vertical motions of the lithosphere during extension and the "necking depth" parameter inferred from kinematic modeling studies, *J. geophys. Res.,* **104**(B10), 23 245–23 254.

Govers, R. & Wortel, M.J.R., 2005. Lithosphere tearing the STEP faults: response to edges of subduction zones, *Earth planet. Sci. Lett.,* **236,** 505–523.

Grunau, H.R., 1981. Worldwide review of seals for major accumulations of natural gas (abstract), *AAPG Bull.,* **65,** 933.

Hall Wallace, M. & Melosh, H.J., 1994. Buckling of a pervasively faulted lithosphere, *Pure appl. Geophys.,* **142,** 239–261.

Hettema, M., Papamichos, E. & Schutjens, P., 2002. Subsidence delay: field observations and analysis, *Oil & Gas Science and Technology – Rev. IFP,* **57**(5), 443–458.

Hol, S., Mossop, A.P., van der Linden, A.J., Zuiderwijk, P.M.M. & Makurat, A.H., 2015. Long-term compaction behavior of Permian sandstones - An investigation into the mechanisms of subsidence in the Dutch Wadden Sea, in *Proceedings of the 49th US Rock Mechanics/Geomechanics Symposium,* American Rock Mechanics Association, San Francisco, CA.

Ketelaar, V.B.H., 2009. *Satellite Radar Interferometry: Subsidence Monitoring Techniques,* Springer.

Lefond, S.J., 1969. *Handbook of World Salt Resources,* Plenum Press.

Li, S., Abe, S., Urai, J.L., Strozyk, F., Kukla, P.A. & van Gent, H., 2012. A method to evaluate long-term rheology of Zechstein salt in the Tertiary, in *Mechanical Behaviour of Salt VII,* pp. 215–220, eds Berest, P., Ghoreychi, M., Hadj-Hassen, F. & Tijani, M., Taylor & Francis Group.

Marketos, G., Govers, R. & Spiers, C.J., 2015. Surface subsidence induced by hydrocarbons extraction, and the potential for time-dependent

ground deformations, in *Proceedings of the 49th US Rock Mechanics/Geomechanics Symposium,* American Rock Mechanics Association, San Francisco, CA, 7 pp.

Melosh, H.J. & Raefsky, A., 1980. The dynamical origin of subduction zone topography, *Geophys. J. R. astr. Soc.,* **60,** 333–354.

Mogi, K., 1958. Relations between the eruptions of various volcanoes and the deformations of the ground surfaces around them, *Bull. Earthquake Res. Inst. Univ. Tokyo,* **36,** 99–134.

Mohriak, W.U., Szatmari, P. & Anjos, S., 2012. Salt: geology and tectonics of selected Brazilian basins in their global context, *Geol. Soc. Lond., Special Publications,* **363,** 131–158.

Montgomery, S.L. & Moore, D.W., 1997. Subsalt play, Gulf of Mexico: a review, *AAPG Bull.,* **81,** 871–896.

Muntendam-Bos, A.G., Kroon, I.C. & Fokker, P.A., 2008. Time-dependent inversion of surface subsidence due to dynamic reservoir compaction, *Math. Geosci.,* **40,** 159–177.

Nagel, N.B., 2001. Compaction and subsidence issues within the petroleum industry: from Wilmington to Ekofisk and beyond, *Phys. Chem. Earth (A),* **26**(1–2), 3–14.

NAM, 2010. Bodemdaling door Aardgaswinning: Statusrapport 2010 en Prognose tot het jaar 2070. Available at: http://www.commissiebodemdaling.nl/files/nam_bodemdalingsrapport2010.pdf, last accessed 4 June 2015.

NAM, 2013. Technical addendum to the winningsplan Groningen 2013: Subsidence, induced earthquakes and seismic hazard analysis in the Groningen Field. Available at: http://www.rijksoverheid.nl/bestanden/documenten-en-publicaties/rapporten/2014/01/17/bijlage-1-analyse-over-verzakkingen-geinduceerde-aardbevingen-en-seismische-risico-s/2-2-a-technical-addendum-to-the-winningsplan-groningen-2013.pdf, last accessed 4 June 2015.

Orlic, B., ter Heege, J. & Wassing, B.B.T., 2011. Assessing the short-term and long-term integrity of top seals in feasibility studies of geological CO_2 storage, in *45th US Rock Mechanics/Geomechanics Symposium,* San Francisco, CA.

Orlic, B. & Wassing, B.B.T., 2013. A study of stress change and fault slip in producing gas reservoirs overlain by elastic and viscoelastic caprocks, *Rock Mech. Rock. Eng.,* **46,** 421–435.

Peck, R., 1969. Deep excavations and tunnelling in soft ground, in *Proceedings of the 7th International Conference on Soil Mechanics and Foundation Engineering,* Mexico City, Sociedad Mexicana de Mecanica, State of the Art Volume, pp. 225–290.

Pinto, F. & Whittle, A.J., 2014. Ground Movements due to Shallow Tunnels in Soft Ground. I: Analytical Solutions, *J. Geotech. Geoenviron. Eng.,* **140**(4), 04013040.

Prij, J., 1991. On the design of a radioactive waste repository, *PhD thesis,* University of Twente, pp. 227, ISBN:90-375-0261-X.

Puzrin, A.M., Burland, J.B. & Standing, J.R., 2012. Simple approach to predicting ground displacements caused by tunnelling in undrained anisotropic elastic soil, *Géotechnique,* **62**(4), 341–352.

Ranalli, G., 1995. *Rheology of the Earth,* 2nd edn, Chapman and Hall.

Rankin, W.J., 1988. Ground movements resulting from urban tunnelling: prediction and effects, in *Engineering Geology Special Publications,* Vol. 4, pp. 79–92, Geological Society.

Schoenherr, J. *et al.*, 2007. Limits to the sealing capacity of rock salt: a case study of the Infra-Cambrian Ara Salt from the South Oman salt basin, *AAPG Bull.,* **91**(11), 1541–1557.

Segall, P., 2010. *Earthquake and Volcano Deformation,* Princeton University Press.

Spiers, C.J. & Carter, N.L., 1998. Microphysics of rocksalt flow in nature, in *Proceedings of the 4th Conference on the Mechanical Behavior of Salt, Trans Tech Publication Series on Rock and Soil Mechanics*, Vol. 22, pp. 115–128, eds Aubertin, M. & Hardy, H.R. Trans Tech Publications, Clausthal, Germany.

Spiers, C.J., Schutjens, P.M.T.M., Brzesowsky, R.H., Peach, C.J., Liezenberg, J.L. & Zwart, H.J., 1990. Experimental determination of constitutive parameters governing creep of rocksalt by pressure solution, in *Deformation Mechanisms, Rheology and Tectonics,* Vol. 54, pp. 215–227, eds Knipe, R.J. & Rutter, E.H., Geological Society of London Special Publication.

Urai, J.L., Schléder, Z., Spiers, C.J. & Kukla, P.A., 2008. Flow and transport properties of salt rocks, in *Dynamics of Complex Intracontinental Basins: The Central European Basin System,* pp. 277–290, eds Littke, R., Bayer, U., Gajewski, D. & Nelskamp, S., Springer-Verlag.

Urai, J.L. & Spiers, C.J., 2007. The effect of grain boundary water on deformation mechanisms and rheology of rock salt during long-term deformation, in *Proceedings of the 6th Conference on the Mechanical Behavior of Salt - Understanding of THMC Processes in Salt,* eds Wallner, M., Lux, K.H., Minkley, W. & Hardy, H.R., Taylor and Francis, London, pp. 149–158.

van Keken, P.E., Spiers, C.J., van den Berg, A.P. & Muyzert, E.J., 1993. The effective viscosity of rocksalt: implementation of steady state creep laws in numerical models of salt diapirism, *Tectonophysics,* **225,** 457–476.

Vasco, D.W., Ferretti, A. & Novali, F., 2008. Reservoir monitoring and characterization using satellite geodetic data: interferometric synthetic aperture radar observations from the Krechba field, Algeria, *Geophysics,* **73,** WA113–WA122.

Verruijt, A., 1996. Complex variable solutions of elastic tunnelling problems, Geotechnical Laboratory, Delft University of Technology. Available at: http://geo.verruijt.net/software/Tunnels.zip, last accessed 4 June 2015.

Yoshikawa, K., 1961. On the crustal movement accompanying with the recent activity of the Volcano Sakurajima, Part 2, *Bull. Disaster Prev. Res. Inst. Kyoto Univ.,* **50,** 1–26.

Yu, Y., Tang, L., Yang, W., Huang, T., Qiu, N. & Li, W., 2014. Salt structures and hydrocarbon accumulations in the Tarim Basin, northwest China, *AAPG Bull.,* **98,** 135–159.

Zymnis, D., Chatzigiannelis, I. & Whittle, A.J., 2013. Effect of anisotropy in ground movements caused by tunnelling, *Géotechnique,* **63**(13), 1083–1102.